

XP008013346

P.D. 21.01.2002

P. 54-58 (5)

## Quantitative OCT Image Correction Using Fermat's Principle and Mapping Arrays

Volker Westphal<sup>1</sup>, Sunita Radhakrishnan<sup>2</sup>, Andrew M. Rollins<sup>1,2</sup>, and Joseph A. Izatt<sup>3</sup>

Departments of <sup>1</sup>Biomedical Engineering and <sup>2</sup>Medicine  
Case Western Reserve University, Cleveland, Ohio  
Department of <sup>3</sup>Biomedical Engineering  
Duke University, Durham, North Carolina

### Abstract

Optical coherence tomography (OCT) is a relatively new developed technique to image tissue microstructure *in vivo* with a resolution of about 10  $\mu$ m. So far, the research has focused on increasing the resolution, increasing the acquisition rate, developing new sample arm scanning techniques, or functional imaging like color Doppler OCT. But one of the main advantages of OCT compared to ultrasound, non-contact imaging, also results in a major image distortion: refraction at the air-tissue interface. Also, applied scanning configurations can lead to deformed images. Both errors prevent accurate distance and angle measurements on OCT images, necessary e.g. for Glaucoma diagnosis in the anterior segment of the eye.

We describe a methodology for quantitative image correction in OCT which includes procedures for correction of arbitrary spatial warping caused by non-uniform axial reference and lateral sample scan patterns, as well as a novel approach for refraction correction in layered media based on Fermat's principle. The de-warping corrections are implemented in real-time by use of pointer (mapping) arrays, while the refraction correction algorithm is more computationally intensive and is performed off-line.

**Keywords:** Optical coherence tomography, OCT, Fermat's principle, scanning configuration, image distortion

### INTRODUCTION

Optical coherence tomography is a relatively new technology, which is capable of micron-scale resolution imaging noninvasively in living biological tissues. Although it is relatively straightforward to use OCT to obtain accurate optical thickness measurements along a given axial scan line in a homogeneous medium, there are many potential applications of OCT in which accurate two-dimensional reconstruction of complex features in layered media are required. One such application is in ophthalmic anterior segment biometry [1], in which not only linear distances but also curvilinear surfaces, interfaces, and enclosed areas must be accurately obtained. OCT is a relatively young technology in which the hardware is still maturing, focusing e.g. on resolution improvements [2], real-time imaging, and functional OCT like color Doppler OCT [3] or polarization sensitive OCT [4, 5]. Meanwhile relatively little attention has been paid to image processing for quantitative image correction.

We describe a methodology for quantitative image correction in OCT which includes procedures for correction of arbitrary spatial warping caused by non-rectangular axial reference and lateral sample scan patterns, as well as a novel approach for refraction correction in layered media based on Fermat's principle. The de-warping corrections are implemented in real-time by use of pointer (mapping) arrays, while the refraction correction algorithm is more computationally intensive and is performed off-line.

XP008013346

## METHODS

Both dewarping and refraction correction transformations are implemented as backward-transformations, meaning we determine for a given position  $P = (x, y)$  in the target image to be displayed the position  $P' = (x', y')$  in the raw data acquired by a digitizer or frame grabber:

$$\begin{aligned} x' &= f_x(x, y) \\ y' &= f_y(x, y) \end{aligned} \quad (1)$$

Implementation of spatial image correction using backward transformations has many advantages. Compared with the forward transformation, the interpolations to obtain the pixel value at non-integer positions is vastly simplified with the backward transformation. Second, the only needs one transformation per target pixel, the optimum. For static transformations (e.g. to correct scan nonlinearities and scan geometry), we pre-calculated spatial look-up-tables, called mapping arrays, to allow real-time display.

## SCAN NONLINEARITY

One important source of spatial warping in real-time OCT systems is sinusoidal axial image nonlinearity due to harmonic motion of the resonant scanner in the reference arm rapid-scan optical delay (Fig. 1A). This source of image warping may be corrected using the inverse transform. Normally the duty cycle  $\eta$  of the acquisition is less than 100%. Therefore the complete scan depth  $A$  has to be calculated from  $\eta$  and the visible scan depth  $d$ .

$$A = \frac{d}{2} \sin^{-1} \left( \frac{\pi \eta}{2} \right). \quad (1)$$

In consequence, the backward transformation can be written as

$$x' = F_{\text{raw}}(x, y) = x \quad (2)$$

$$y' = F_{\text{raw}}(x, y) = \frac{d}{\pi \eta} \arcsin \left( \frac{y}{A} \right). \quad (3)$$

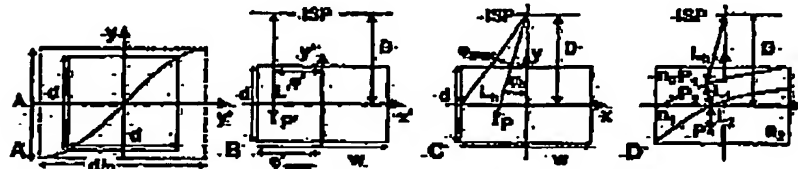


Fig. 1. A) Correction of nonlinear axial scanning B) Coordinate system of the raw image (raw image). C) Target coordinate system in a homogeneous medium; D) Refractive interfaces in the sample after ray paths.

Abbreviations:  $A$ : full amplitude of depth scan,  $\eta$ : axial duty cycle of acquisition,  $D$ : distance on axis to image of scanning pivot (ISP),  $w$ : width,  $d$ : depth of acquired image,  $x'$ : primed coordinates in raw data, unprimed in target image,  $P$  and  $P'$ : corresponding points in target and source image,  $\alpha$ : scan angle,  $\rho_{\text{max}}$ : extreme scan angle in the vertical center of the image,  $L$ : distance from  $P$  or  $P'$  to the ISP,  $L_1$ ,  $L_2$ : partial distances in inhomogeneous sample with the indices of refraction  $n_1$  and  $n_2$ ,  $L = L_1 + L_2 + L_3$ .

## NON-TELEGENTRIC SCANNING

To correct for geometric image distortions due to non-telecentric scanning, the coordinate systems for the raw and target images are defined in terms of the scan geometry (Fig. 1B,C). We assume the OCT image is formed using a sample arm probe, which incorporates a rotating mirror scanner [2]. The origin for both systems is in the center of the image.  $x'$  is linear with acquisition time and thereby with the lateral scanning mirror movement. The center of the field of view (FOV, having width  $w$  and depth  $d$ ) is a distance  $D$  from the scanning pivot (SP) or an image of the sample pivot (ISP), depending upon the internal details of the sample arm probe. For positive or negative  $D$ , scans diverge or converge, respectively. For telecentric scans  $D$  approaches infinity, but for any real system, this can always be approximated by a large  $D$ . The target pixel position  $P$  can also be defined in polar coordinates  $(\phi, L)$ , with the scanning angle  $\phi$  in the FOV and the distance  $L$  from ISP to  $P$  (Fig. 1B,C). For a homogeneous sample without refraction (denoted by subscript  $h$ ),  $\phi$  and  $L$  are given by

$$g_1(x, y) = \text{atan}(x \text{AD} - y), \quad (4)$$

804

$$L_1(x, y) = D - \sqrt{x^2 + (D-y)^2} \quad (5)$$

The scanning angle to reach the extreme of the FOV at the center plane is given by  $\varphi_{\text{ext}} = \varphi_0 (w/2, 0)$ . In the rectangular array of acquired data, the scan angle  $\varphi'$  in the FOV is linear with position  $x'$ :  $\varphi'(x', y') = 2x' \varphi_{\text{ext}} / w = x' / D$ , while the distance between ISP and  $P'$  is  $L'(x', y') = D - y'$ . Since  $\varphi = \varphi'$ ,  $L = L'$ , and  $\varphi_{\text{ext}} = \varphi'_{\text{ext}}$ , the complete backward transformations are given by:

$$x' = F_{\text{sh}}(x; y) = \arctan\left(\frac{x}{D - v}\right) \cdot D \quad (6)$$

$$y' = F_{+}(x, y) = D - \sqrt{x^2 + (D - y)^2} \quad (7)$$

#### REFRACTION CORRECTION

In many biological samples, significant refraction of OCT light occurs at smooth refractive index boundaries, for example the anterior and posterior surfaces of the cornea. A forward transformation to correct for refraction could use Snell's law to calculate the target (display) pixel given the raw data pixel. However, the forward transformation would result in blank or double-valued target pixels unless time-consuming interpolation and renormalization algorithms are implemented for each update of the acquired image. For the backward transformation, a novel approach is to apply Fermat's principle which states that the light will follow the minimum optical path length through all index boundaries between the sample probe tip and the target location (Fig. 3). In this case,

$$L(x_1, y_1, x_{M1}, y_{M1}, x_{A2}, y_{A2}) = L_1(x_1, y_1) + L_2(x_{M1}, y_{M1}, x_{A2}, y_{A2}) + L_3(x_{A2}, y_{A2}, x_1, y_1) \quad (3)$$

must be minimized. We have implemented this idea as a minimization procedure in which discrete tissue index boundaries are interactively identified, fit to a spline curve, and used to find the minimum optical path. Fermat's principle has previously been used in geophysics [6] and astrometry [7].

## RESULTS

Both spatial dewarping corrections and refraction corrections were implemented on a real-time OCT system designed for anterior segment imaging using a hand-held probe. Axial sinusoidal dewarping and lateral divergence corrections were implemented at up to 16 frames/sec using a mapping array.

To test the accuracy of the image corrections we used a metal mesh of 317  $\mu\text{m}$  line spacing as a test-object. Mounted on a linear translator in front of the probe, it was imaged at several axial positions. For the test of the nonlinear scan correction the axial offset was 100  $\mu\text{m}$ . Fig. 2A) shows the measured location of the central wire, before and after dewarping. As a result, maximum position error could be reduced from 176  $\mu\text{m}$  to 4.6  $\mu\text{m}$ . The residual appears to have a 5<sup>th</sup> order term. However, this term can be neglected, since it is below the axial resolution limit determined by the light source.

Fig. 2B shows an overlay of images of the grid, taken at an axial offset of 500  $\mu\text{m}$  (exception: top 400  $\mu\text{m}$  and bottom 300  $\mu\text{m}$ ). This image is already corrected for nonlinear axial scanning. The error vectors compared to the known gridline positions before and after the non-telecentric scan correction are displayed in Fig. 2C. The length of the latter is increased tenfold. The maximum error could be reduced from 304 to 17  $\mu\text{m}$ .

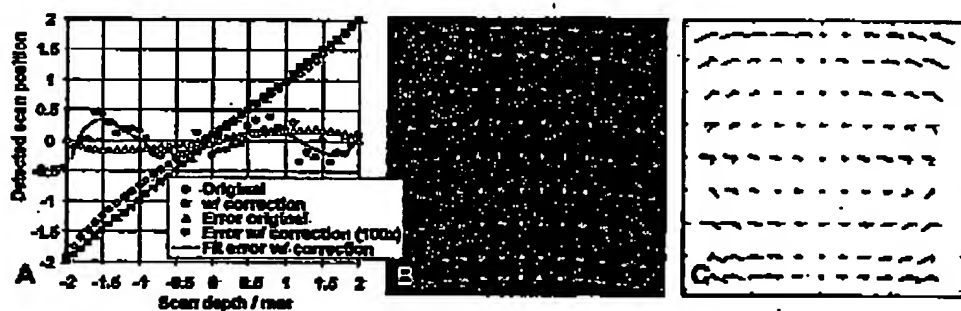


Fig. 2. A) Distortion correction of surface axial scanning. B) Overlay of calibrated images acquired at different axial positions, each image averaged over 50 frames, corrected for nonlinear axial scanning. C) Residual error vectors *in situ* (thin line), without correction (thick line), and with aberration correction (length  $\times 10$ ).

As a last test, we demonstrate the operation of the Fermat's principle algorithm on a phantom (a drop of Intralipid on a glass slide). Fig. 3A is distorted in multiple ways: 1) non-telecentric scanning bends the glass side 2) below the drop the glass slide is bulged to the bottom 3) the thickness of the slide is too high. All three are corrected in Fig. 3B, the maximum flatness deviation of the slide surfaces is 10 (top) and 13  $\mu\text{m}$  (bottom). The thickness of the slide could be determined with a precision of 1 %. Refraction correction was performed off-line on digitally saved images, primarily necessitated by the need for interactive identification of index boundaries in the tissue.

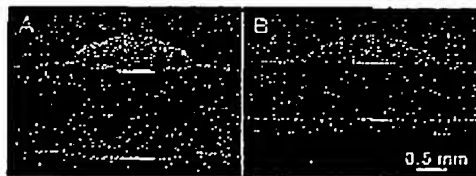


Fig. 3. A) Uncorrected image of an Intralipid<sup>®</sup> drop on a coverlip; B) corrected image

For the diagnosis of acute angle-closure glaucoma OCT can be a valuable tool, because it can image the angle through the opaque sclera. Compared to ultrasound biomicroscopy no contact with the eye is required, dramatically increasing the patient comfort. But the substantial changes in angle appearance (Fig. 4) during the different processing steps illuminate the need of these correction to accurately access this angle.

This study was partially funded by the National Institutes of Health (EY13015).

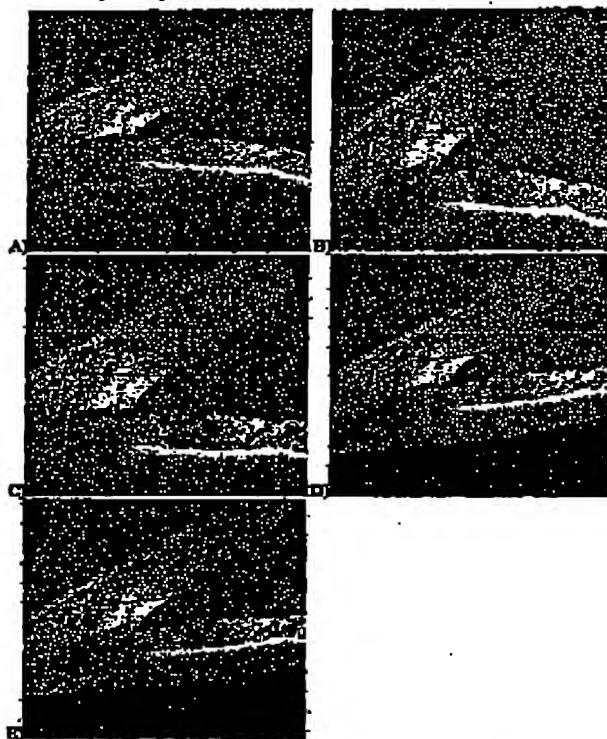


Fig. 4: OCT images of the temporal anterior chamber angle of a human eye, imaged *in vivo*, at 8 frames/sec, at different stages of quantitative image correction: A) raw image, B) removal of nonlinear reference mirror movement, C) correction of divergence lateral scan due to handheld OCT probe, D) corrected for refraction at the air-cornea boundary ( $n_{air} = 1.39$ ), E) additional correction for refraction at the endothelium-aqueous boundary ( $n_{aqueous} = 1.33$ ). The surfaces of the corneal epithelium and endothelium were drawn with user input and fitted to a spline.

#### References

1. Radhakrishnan, S., Rollins, A. M., Roth, J. E., Yazdani, S., Westphal, V., Bardenstein, D. S., and Izquierdo, J. A. Real-time optical coherence tomography of the anterior segment at 1310 nm. *Archives of Ophthalmology*. In press.
2. Drexler, W. et al. "High-resolution ophthalmic optical coherence tomography," *Nature Medicine* 7 (4): 502-507 (2000)
3. Yazdani, S., A. M. Rollins, and J. A. Izquierdo, "Imaging and velocimetry of the human retinal circulation with color Doppler optical coherence tomography," *Opt. Lett.* 25 (19): 1448-1450 (2000)
4. Sezen, C. H. et al. "High-speed fiber-based polarization-sensitive optical coherence tomography of *in vivo* human skin," *Opt. Lett.* 25 (18): 1355-1357 (2000)
5. Roth, J. E. et al. "Simplified method for polarization-sensitive optical coherence tomography," *Opt. Lett.* 26 (14): 1069-1072 (1 A.B.)
6. Moser, T. J. "SHORTEST-PATH CALCULATION OF SEISMIC RAYS," *Geophysics* 56 (1): 59-67 (1991)
7. Perlick, V. "Fermat's principle, Morse theory and applications to the gravitational lens effect," *Nonlinear Analysis-Theory Methods & Applications* 30 (1): 617-625 (1997)